Selection Metric for Photovoltaic Materials Screening Based on Detailed-Balance Analysis

Beatrix Blank,[1] Thomas Kirchartz,[1,2] Stephan Lany,[3] and Uwe Rau[1]
[1]IEK5-Photovoltaics, Forschungszentrum Jülich, 52425 Jülich, Germany
[2]Faculty of Engineering and CENIDE, University of Duisburg-Essen, Carl-Benz-Strasse 199, 47057 Duisburg, Germany
[3]National Renewable Energy Laboratory, Golden, Colorado 80401, USA
(Received 15 March 2017; revised manuscript received 27 June 2017; published 31 August 2017)

The success of recently discovered absorber materials for photovoltaic applications has been generating increasing interest in systematic materials screening over the last years. However, the key for a successful materials screening is a suitable selection metric that goes beyond the Shockley-Queisser theory that determines the thermodynamic efficiency limit of an absorber material solely by its band-gap energy. In this work, we develop a selection metric to quantify the potential photovoltaic efficiency of a material. Our approach is compatible with detailed balance and applicable in computational and experimental materials screening. We use the complex refractive index to calculate radiative and nonradiative efficiency limits and the respective optimal thickness in the high mobility limit. We compare our model to the widely applied selection metric by Yu and Zunger [Phys. Rev. Lett. **108**, 068701 (2012)] with respect to their dependence on thickness, internal luminescence quantum efficiency, and refractive index. Finally, the model is applied to complex refractive indices calculated via electronic structure theory.

DOI: 10.1103/PhysRevApplied.8.024032

I. INTRODUCTION

Because of the wide variety of potential absorber materials for photovoltaic applications, including organic and inorganic materials as well, are organic inorganic compounds. Like the recently developed perovskite solar cells, there has been growing interest in recent years to find new photovoltaic absorber materials via computational but also experimental materials screening [1–14]. The purpose of materials screening is to identify promising materials for more in-depth investigations based on a limited amount of information on the material. For a given purpose, such as photovoltaics, it is, therefore, crucial to decide what information on a material is needed to make well-informed decisions in a finite amount of time. This requires a suitable "selection metric" for promising absorber materials for photovoltaic applications that goes beyond the radiative efficiency limit as calculated by Shockley and Queisser (SQ) [15]. The SQ approach describes a solar cell exclusively by an external property: the steplike absorption $A(E) = \Theta(E - E_g)$. Thus, the radiative efficiency limit depends on one parameter only: the band-gap energy E_g.

It is apparent that exclusively considering the band-gap energy of a material is not sufficient to estimate its potential as an absorber material. Numerous other properties such as the mobility [16,17], the absorption coefficient [18,19], the charge-carrier lifetime [18–20], and the luminescence quantum efficiency [21–27] have an enormous effect on a solar cell's performance. Hence, there have been various studies to calculate a more realistic efficiency limit beyond the SQ limit for different technologies and assumptions [18,19,28–36].

One of the first and may be most prominent examples of such a selection metric proposed for computational materials screening was presented by Yu and Zunger [37] in 2012 and has been widely used to estimate efficiency limits in the last years [38–49]. In their paper, they proposed a "spectroscopic limited maximum efficiency" (SLME) selection metric that aims to calculate efficiency limits for non-step-like absorption coefficients beyond the radiative limit. They calculated the efficiency in the high mobility limit using absorption coefficients simulated via electronic structure theory. While the SLME takes nonradiative recombination into account, the paper does not distinguish between internal Q_i and external luminescence yield Q_e; i.e., the number of photons generated in the device via radiative recombination are set equal to the number of photons that subsequently escape the device, and it is, therefore, only correct in the limit of perfect light outcoupling, a limit that does not apply to realistic devices.

The present paper proposes a modified selection metric based on Ref. [24] that is detailed-balance compatible and takes the effects of light outcoupling, photon recycling, and nonradiative recombination into account. As illustrated by Fig. 1, the complex refractive index, the device thickness, and the light-trapping structure represent the *minimum* parameter set needed for a physically consistent approximation of the efficiency potential of a photovoltaic absorber material defined by bulk material properties and not by the band-gap energy only. This step takes us from a description of the solar cell as a *surface* specified by a step-function-like absorptance in the SQ approach to a solar cell specified by *bulk* properties. This minimum parameter set allows us

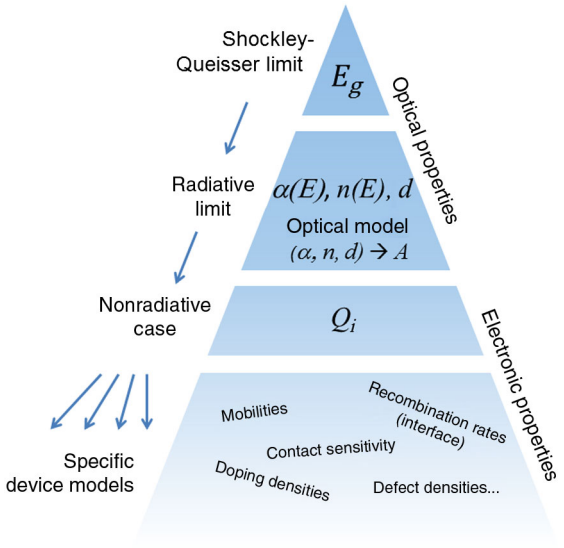

FIG. 1. The SQ limit is derived using an approximation that is parametrized by the band-gap energy E_g only. Steps for more detail must be undertaken in the order of top to bottom. Any model describing the radiative limit as a function of material properties must contain the absorption coefficient $\alpha(E)$ and the refractive index $n(E)$ as well as assumptions on the device thickness and an optical model for light trapping. The next step involves nonradiative recombination, i.e., an internal luminescence quantum efficiency $Q_i < 1$. Generic device models considering finite mobilities, interface recombination, or contact selectivity must involve the first two steps in order to be compatible with the SQ approach. Note that the standard device simulations for real photovoltaic devices usually involve hundreds of material-specific parameters.

to calculate the (nonstep function) absorptance and herewith the radiative limit; see Fig. 1. We emphasize that there is no other intermediate step possible, and any sophistication of the SQ approach needs to consider at least this parameter set in order to be physically consistent.

The next step towards more detail in this top-down approach is the inclusion of nonradiative recombination in terms of an internal luminescence quantum efficiency leading us to a generic nonradiative case. Notably, we shift then from optical properties to electronic properties. Within the present paper, we restrict ourselves to this level of detail, whereas one might think about the selectivity of contacts [50] and the influence of carrier mobilities [16] as the logical next levels of detail, which are still far more generic than detailed device models.

We note that the procedure proposed here corresponds to the way, e.g., Tiedje *et al.* [51] have calculated the efficiency limit for crystalline silicon solar cells [51], how Marti *et al.* [52] have explained the importance of photon recycling, how Mattheis *et al.* [16] have calculated the radiative mobility limits of photovoltaic energy conversion, and how the impact of a direct or indirect band gap on the efficiency potential of metal-halide perovskites was evaluated [53]. Thus, the issue of the present paper is to systematically describe what all these authors (and many others) have done right and therewith to establish a canonical, detailed-balance-compatible top-down approach. This approach serves as a guideline, and finally, a recipe, on how to conduct and correctly interpret first-principles calculations for photovoltaic materials.

We demonstrate this method by applying it to different materials whose complex refractive index is calculated by first-principles calculations in the so-called GW approximation [54] (where G is the Greens function and W is the screened Coulomb potential) in the radiative limit (internal luminescence quantum efficiency $Q_i = 1$). In addition, we highlight how sensitive the efficiency limit reacts on nonradiative recombination, i.e., when Q_i is reduced. The approach proposed here will be useful both for computational materials screening in photovoltaics and for experimental materials screening where properties of absorber layers are used to determine the efficiency potential of a certain material class [20,55,56].

II. THEORY

A. Shockley-Queisser limit

Shockley and Queisser determined thermodynamic efficiency limits based on the principle of detailed balance. The short-circuit current in the SQ limit is written as

$$J_{\mathrm{SC}} = q \int_0^\infty A(E)\phi_{\mathrm{Sun}}(E)dE, \tag{1}$$

where E is the energy, q the elementary charge, and the absorptance $A(E)$ is assumed to be a step function at the band-gap energy E_g defined as $A(E) = 0$ for $E \leq E_g$ and $A(E) = 1$ for $E > E_g$. Whereas in the original paper by Shockley and Queisser, the spectrum of the Sun is approximated by the blackbody spectrum at temperature $T = 6000$ K, in this work, we use the AM1.5g [57] spectrum, as it is common nowadays. The radiative saturation current can be calculated via

$$J_0^{\mathrm{rad}} = q \int_0^\infty \pi A(E)\phi_{\mathrm{BB}}(E, T = 300\ \mathrm{K})dE. \tag{2}$$

The blackbody spectrum at temperature T is given by $\phi_{\mathrm{BB}}(E,T) = 2E^2h^{-3}c^{-2}[\exp(E/kT) - 1]^{-1}$, where h denotes the Planck constant, c the velocity of light in vacuum, and k the Boltzmann constant. Assuming an ideality factor of $n_{\mathrm{id}} = 1$, the efficiency limit η (in the radiative limit η^{rad}, i.e., internal luminescence quantum efficiency $Q_i = 1$) is given by

$$\eta^{(\mathrm{rad})} = \frac{\max_V \left(V \left\{ J_{\mathrm{SC}} - J_0^{(\mathrm{rad})} \left[\exp\left(\frac{qV}{kT}\right) - 1 \right] \right\} \right)}{\int_0^\infty E\phi_{\mathrm{Sun}}(E)dE}, \tag{3}$$

where V is the voltage of the solar cell.

TABLE I. Internal vs external parameters. Note that the radiative and nonradiative recombination rates are defined here as the recombination rates in thermodynamic equilibrium.

Internal parameter		External parameter	
Absorption coefficient	α	$1-\exp(-2\alpha d)=A(E)$ (e.g., flat cell, Lambert-Beer approximation)	Absorptance
Nonradiative recombination rate	R_0^{nrad}	$q\int R_0^{\mathrm{nrad}}dx=J_0^{\mathrm{nrad}}$	Nonradiative saturation current density
Radiative recombination rate	R_0^{nrad}	$p_e q\int R_0^{\mathrm{rad}}dx=J_0^{\mathrm{rad}}$	Radiative saturation current density
Internal (luminescence) quantum efficiency	Q_i	$p_e Q_i/[1+(p_e-1)Q_i]=Q_e$	External luminescence quantum efficiency

Shockley and Queisser consider only one material property—the band-gap energy E_g—by assuming a step-like absorption. However, the simplicity achieved by the step function forces Shockley and Queisser to implicitly assume that the solar-cell absorber is both infinitely thick (to achieve the step function) and infinitely thin at the same time (because perfect charge-carrier collection is another inherent assumption of Shockley and Queisser) [58]. Therefore, a generalization of the SQ theory [31–33] is needed to adapt this approach to a realistic scenario and finally define a suitable selection metric for computational and experimental materials screening.

B. Extended detailed-balance theory

The original SQ theory is, in general, straightforward to generalize because Eqs. (1)–(3) are also valid for non-step-function-like absorptances, thereby allowing for the calculation of the radiative efficiency limit of real materials [18,19,33,35,55]. For computational materials screening, however, we have to go one step further by connecting the internal material properties with external device properties. This is often not implemented correctly and has led to confusion and mistakes in the past [37–49]. The internal and external parameters used in the scope of this work are listed in Table I as well as the equations that connect an internal parameter with its external counterpart.

One example of an internal parameter is the complex refractive index, which describes the optical properties of the material. The corresponding external parameter is the absorptance $A(E)$ which depends on, e.g., the complex refractive index (or the absorption coefficient), the thickness, and the scattering properties of the interfaces (flat or textured). Another example is the recombination rates and the recombination currents. Whereas the rates describe the recombination per volume and time, the currents are the integrated rates per area and time, and in the case of the radiative recombination current, they also include the percentage of photons that are coupled out of the device and not reabsorbed in the solar cell. Therefore, the recombination currents and, consequently, the external luminescence quantum efficiency Q_e depend on the outcoupling and optical properties of the device, whereas the internal quantum efficiency Q_i depends primarily on the properties of the material (electron-photon and electron-phonon coupling). Note that in case of geometric features on the size of the wavelength, interference effects can modify the spontaneous emission rate and thereby Q_i (Purcell effect) [59,60].

It is clear that materials screening provides internal parameters, while efficiency estimates require external properties. Any sensible selection metric, therefore, has to find a way to self-consistently and correctly calculate the external parameters from internal parameters. Figure 2 illustrates the "internal material world" and the "external device world" where the solar cell is treated as a black box with optical and electrical input and output. The connection between the internal and external picture is light incoupling and outcoupling, i.e., optics, and is described consistently with the principle of detailed balance in the following.

At first, the external property—the absorptance $A(E)$—needs to be computed from the absorption coefficient $\alpha(E)$, a volume-related internal property of the photovoltaic absorber material. The calculation of $A(E)$ requires assumptions on the thickness d and on the applied light-trapping scheme [18,61]. In this work, we apply two different light-trapping schemes. The first model represents the case of a solar cell with flat front and back surfaces. For simplicity, the reflectance at the front surface is set to zero, and the reflectance at the back is assumed to be unity. The complex refractive indices of the materials are considered to be homogeneous and isotropic. Moreover, we neglect any interference effects such as resonator modes. For a more detailed description and the respective equation, see the Supplemental Material [61]. The second model is identical with respect to the assumptions on reflectance, optical isotropy, and homogeneity, but it assumes a Lambertian scatterer at the front surface. In this case, we use the analytical solution via the exponential integral function introduced by Green [62].

A similar step from volume to surface properties with careful distinction between internal and external parameters is required for the description of recombination. Here, the internal volume parameters are the radiative and nonradiative recombination rates R^{rad} and R^{nrad} defining the internal luminescence quantum efficiency as follows:

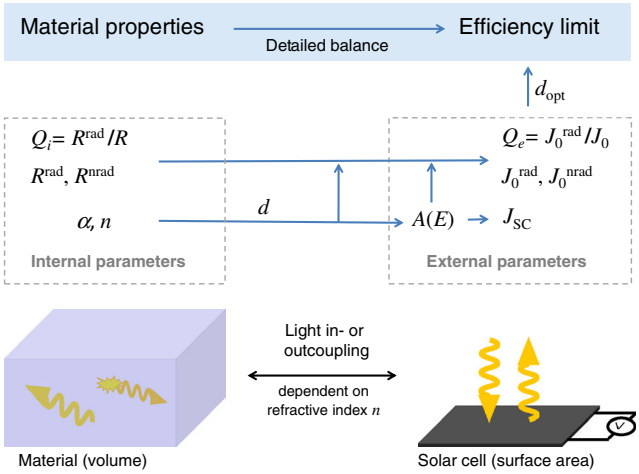

FIG. 2. Illustration of the internal material description (via volume-related material properties) and the external device description (via area-related cell properties) of a solar cell. On the left, the path of the photons inside the volume of the cell and their interaction with electron-hole pairs are considered. On the right side, the light and current are described as input and output parameters of a solar-cell device. For the calculation of the efficiency limit of a device from material properties (absorption coefficient α, refractive index n, radiative recombination rate R^{rad}, nonradiative recombination rate R^{nrad}, internal luminescence quantum efficiency Q_i) towards external variables (short-circuit current density J_{SC}, radiative saturation current density J_0^{rad}, nonradiative saturation current density J_0^{nrad}, external luminescence quantum efficiency Q_e), these two descriptions have to be carefully connected. The maximum device efficiency is obtained by assuming a specific light-trapping scheme and optimizing the cell thickness d.

$$Q_i = \frac{R^{rad}}{R^{rad} + R^{nrad}}. \tag{4}$$

In Secs. III and IV, we assume for simplicity that the radiative and nonradiative recombination rates show the same voltage dependence, i.e., $R^{rad}/R^{nrad} = R_0^{rad}/R_0^{nrad}$. The external surface property—the saturation current densities—are related to the recombination rates as follows:

$$J_0 = J_0^{nrad} + J_0^{rad} = q\int R_0^{nrad}dx + p_e q\int R_0^{rad}dx. \tag{5}$$

Note that the integral $\int dx$ through the depth of the absorber material connects the nonradiative recombination rate R_0^{nrad} in the thermodynamic equilibrium directly with the nonradiative saturation current J_0^{nrad}, whereas the emission probability p_e of the generated photon has to be considered in the case of radiative recombination. As mentioned before, we consider the refractive index to be isotropic and position independent and neglect the interference effects. In this approximation, the van Roosbroeck–Shockley equation describes the radiative recombination rate R^{rad} as a function of n, α, and ϕ_{BB} and combine it with Eq. (2), which yields the quantity p_e,

$$p_e := \frac{J_0^{rad}/q}{\int R_0^{rad}dx} = \frac{\int A(E)\phi_{BB}(E)dE}{4d\int n^2(E)\alpha(E)\phi_{BB}(E)dE} \tag{6}$$

for nonconcentrating solar cells [24]. The emission probability p_e is the factor that connects the internal description of a recombination rate R^{rad} to the external description of a current density J_0^{rad}. This factor depends on the refractive index, i.e., $p_e(n)$. Therefore, we see that we need to consider the refractive index $n(E)$ in addition to the absorption coefficient $\alpha(E)$ for a consistent description of the solar-cell behavior from internal to external properties even if the Lambert-Beer approximation ($A \approx 1 - e^{-2d\alpha}$) is used where $n(E)$ is not needed to calculate the absorptance A. This dependence on the refractive index can be explained intuitively by the influence of total internal reflection and subsequent reabsorption ($p_e \leq 1/n^2$) in the absorber material; see Eq. (6).

However, in the widely applied selection metric proposed by Yu and Zunger (SLME), the refractive index is neglected. Here, an external property—the fraction of radiative electron-hole recombination current $f_r = J_0^{rad}/J_0$—is approximated by $f_r = \exp[(E_g - E_g^{DA})/kT]$, where E_g^{DA} is the dipole-allowed transition energy that is calculated by electronic structure theory. Therefore, the authors derive the external parameters (the ratio of the current densities) from the internal parameters (the band-gap-energy difference $E_g - E_g^{DA}$) without taking the refractive index into account (see Ref. [61], Fig. S2). This is in contradiction to fundamental laws of physics given $Q_i \neq 1$, as outlined above. For a more detailed description and discussion of the SLME, see the Supplemental Material [61]. To show the implications of the negligence of the refractive index, we systematically compare our model to SLME in the following section. For this purpose, we consider SLME not as a method that determines the efficiency limit for a fixed thickness and a fixed f_r given by the band-gap differences but rather as a model that describes a way to calculate the efficiency limit of a device starting from internal material properties. Also, we do not follow the original SLME approach of using the band-gap difference as a way of estimating nonradiative recombination. In reality, the nonradiative rate does not just depend on the optical properties of the perfect material but on the presence of imperfections that act as recombination centers. Therefore, we instead use the internal (luminescence) quantum efficiency Q_i as an adjustable parameter, which corresponds to taking f_r as an adjustable parameter in the SLME approach.

III. DISCUSSION OF MODELS AND PARAMETERS

The influence of the internal quantum efficiency Q_i, the refractive index n, and the thickness d on the efficiency limit is discussed for both models in this section in order to understand the dependences on these parameters and

the resulting difference in the calculated efficiency limits. This systematic study of two exemplarily designed model absorption coefficients in combination with three freely adjustable parameters, e.g., d, Q_i, and n, motivates the selection metric that we introduce in Sec. IV.

Up to this point, we have learned that we need to know (i.e., compute and/or measure) the absorption coefficient *and* refractive index of a photovoltaic absorber material as *necessary* input for a consistent evaluation of its prospective photovoltaic efficiency limit. Moreover, the step from treating a solar cell in terms of a mere surface with the property of an absorptance towards a material volume-related model requires taking the thickness into account. In the first part of this section, we systematically investigate the influence of the cell's thickness on the predicted efficiency potential with the help of model absorption coefficient curves defined by

$$\alpha = \begin{pmatrix} 0 & \text{for } E < E_0, \\ \alpha_0 \exp\left(\frac{E-E_g}{E_{\mathrm{ch}}}\right)\sqrt{\frac{E_{\mathrm{ch}}}{2\exp(1)kT}} & \text{for } E_0 \le E < E_g + \frac{E_{\mathrm{ch}}}{2}, \\ \alpha_0\sqrt{\frac{E-E_g}{kT}} & \text{for } E \ge E_g + \frac{E_{\mathrm{ch}}}{2}. \end{pmatrix} \tag{7}$$

For photon energies $E \ge E_g + (E_{\mathrm{ch}}/2)$, the absorption coefficient follows the square-root law of a direct semiconductor [63], for $E < E_g + (E_{\mathrm{ch}}/2)$, we describe the absorption as an exponential band tail with Urbach energy [64] E_{ch}, and for all energies below the cutoff energy E_0, the absorption is set to zero. The cutoff energy is motivated by the unavoidable experimental and computational limitations in the determination of α in reality.

Figure 3 depicts the two model absorption coefficients that are used in this work as well as the renowned curve of the SQ efficiency limit over band-gap energy E_g (black dashed line). We choose one absorption coefficient with a band-gap energy of $E_g = 1.0$ eV and a cutoff energy of $E_0 = 0.9$ eV (red) and another one with $E_g = 1.5$ eV and $E_0 = 1.4$ eV (blue). The band-gap energies as well as the cutoff energies are selected in a way that they are either both below or above the two local maxima of the SQ limit. The motivation for this specific choice of energy values becomes clearer in the following discussion of the optimal absorber thickness. The tail slope is in both cases equal to $E_{\mathrm{ch}} = 0.5kT$, a reasonable value for common solar-cell materials [65]. The scaling factor α_0 can vary strongly for different materials, but the absolute value is of no importance in the following discussion of our results, as we refer only to normalized thicknesses $\alpha_0 d$ in this paper. For the sake of simplicity, we show the absorption coefficients in Fig. 3 exemplarily for $\alpha_0 = 10^5/\mathrm{cm}$.

Figure 4(a) shows the efficiency as a function of normalized thickness $\alpha_0 d$ for these two sample materials in the radiative limit ($Q_i = 1$) for flat devices. For devices

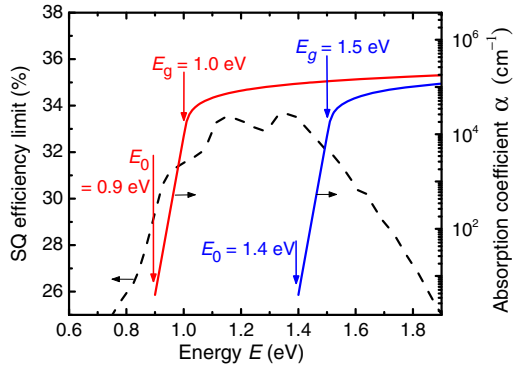

FIG. 3. Two model absorption coefficients versus energy. One absorption coefficient curve (red) is chosen so that both the band-gap energy $E_g = 1.0$ eV and the cutoff energy $E_0 = 0.9$ eV are below the maxima of the SQ efficiency limit (black dashed). The other one (blue) with $E_g = 1.5$ eV and $E_0 = 1.4$ eV is only nonzero for energies above 1.35 eV (second maximum of SQ). In both cases, the characteristic energy of the tail is set to $E_{\mathrm{ch}} = \frac{1}{2}kT$.

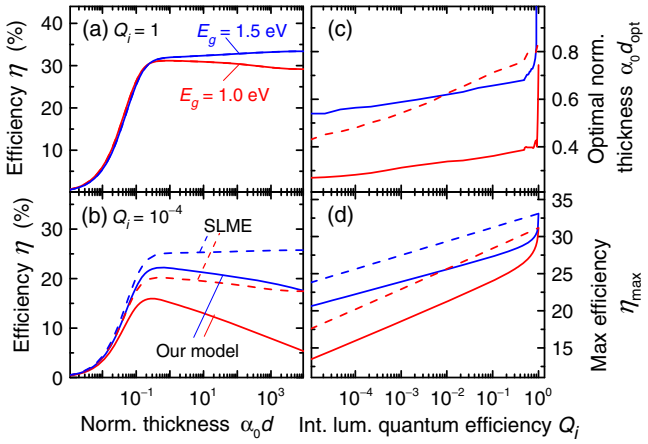

FIG. 4. Efficiency over normalized thickness $\alpha_0 d$ for the model systems $E_g = 1.0$ eV (red) and $E_g = 1.5$ eV (blue). The corresponding absorption coefficients are introduced in Fig. 3; the refractive index is set to 3.5. (a) In the radiative limit, $E_g = 1.0$ eV reaches maximum efficiency at an optimal normalized thickness of $\alpha_0 d_{\mathrm{opt}} \approx 0.7$. In contrast, in the case of $E_g = 1.5$ eV, the efficiency approaches its maximum at infinite thickness. (b) For $Q_i = 10^{-4}$, the efficiencies as calculated with SLME (dashed lines) and our model (solid lines), which takes the refractive index into account, are seen to deviate from one another. The difference in the two models lead to differences in (c) the optimal thickness for all $Q_i \neq 1$, as well as (d) the absolute maximal achievable efficiencies η_{max}, which are significantly overestimated by SLME. Note that in the case of $E_g = 1.0$ eV, the SLME does not predict an optimal thickness, whereas our model always leads to an optimal efficiency for $d \neq \infty$ (given that $Q_i \neq 1$).

with a Lambertian scatterer as the front surface, see Fig. S3 in the Supplemental Material [61]. In the case of $E_g = 1.0$ eV (red), the maximum efficiency is reached at a finite normalized thickness of $\alpha_0 d_{\mathrm{opt}} \approx 0.7$. In contrast, in the case of $E_g = 1.5$ eV (blue), the efficiency approaches its maximum at infinite thickness. A monotonic increase in efficiency with thickness for the latter case can be explained by the fact that both E_g and E_0 are above the energy of the maxima of the SQ limit. Making the absorber thicker and thicker leads to an absorption that is closer and closer to a steplike absorption at E_0. As the SQ limit monotonically decreases from 1.4 to 1.5 eV, the maximum efficiency for the sample system with $E_g = 1.5$ eV and $E_0 = 1.4$ eV increases with increasing thickness. The efficiency asymptotically reaches the efficiency of the SQ limit at 1.4 eV, $\eta^{\mathrm{SQ}}(E_g = 1.4\ \mathrm{eV}) = \eta^{\mathrm{rad}}(d = \infty)|_{E_0 = 1.4\ \mathrm{eV}} \approx 33\%$. Following this reasoning, all absorption coefficients with a cutoff energy higher than 1.33 eV—the energy of the second maximum of the SQ limit—reach their maximum efficiency at infinite thickness. The gain in short-circuit current with increasing thickness is, in those cases, higher than the loss in open-circuit voltage.

The situation is different for band-gap energies below the energy of the SQ maxima. For the sample absorption coefficient with $E_g = 1.0$ eV (red line), the efficiency for infinite thickness is still equal to the SQ limit of the respective cutoff energy: $\eta^{\mathrm{SQ}}(0.9\,\mathrm{eV}) = \eta^{\mathrm{rad}}(d = \infty)|_{E_0 = 0.9\,\mathrm{eV}}$. However, this limit $\eta^{\mathrm{SQ}}(0.9\ \mathrm{eV})$ is lower than the SQ limit of its corresponding band-gap energy $\eta^{\mathrm{SQ}}(1.0\ \mathrm{eV})$. Therefore, the $\eta^{\mathrm{rad}}(d)$ curve increases until it reaches its maximum of $\eta^{\mathrm{rad}}(d_{\mathrm{opt}}) = 31.17\%$ and finally decreases asymptotically towards $\eta^{\mathrm{SQ}}(0.9\ \mathrm{eV})$ for infinite thickness. This shows that apparent subtleties of the optical data (namely, the cutoff energy E_0, the photon energy of the first data point with $\alpha > 0$) become quite important when looking for the optimum thickness in the radiative limit.

The graph drastically changes when we assume an internal luminescence quantum efficiency of $Q_i = 10^{-4}$; see Fig. 4(b). In the case $Q_i < 1$, the efficiencies calculated from our model (solid lines) and the SLMEs (dashed lines) deviate from one another. In the case of $E_g = 1.0$ eV (red), both models predict similar optimal thicknesses. The absolute maximum efficiency, however, is about 20% highly overestimated by SLME in comparison to our model that predicts an efficiency limit of about 16%. Note that in the case of $E_g = 1.5$ eV (blue), not only the maximum efficiencies deviate strongly, but the curves show a qualitatively different behavior. If one neglects the refractive index (SLME, dashed blue line), the efficiency-over-thickness curve does not exhibit a global maximum anymore. To explain the observed differences between the two approaches, we take a closer look at the equations introduced in Sec. II.

The short-circuit currents in both models follow directly from $J_{\mathrm{SC}} = q \int A \phi_{\mathrm{Sun}} dE$ and are, therefore, independent of Q_i. The saturation current J_0 scales with $1/Q_i$ in the SLME model, which leads to the same normalized $J_0(d)$ curves for $Q_i = 1$ and $Q_i = 10^{-4}$. Therefore, J_0 saturates for large thicknesses for all $Q_i \neq 1$, just like it saturates in the radiative limit. This leads to efficiencies greater than 0% for infinite thickness for all $Q_i \neq 1$, which is physically unreasonable. In our model, on the other hand, the outcoupling efficiency p_e decreases with thickness, which leads to a linear increase in J_0 for sufficiently large thicknesses due to the nonradiative term. Consequently, J_0 does not saturate for $Q_i < 1$, and our model predicts an efficiency of 0% for infinite thickness, as one expects.

Figure 4(c) shows the effect of the internal luminescence quantum efficiency on the optimal normalized thickness. The optimal thicknesses for $E_g = 1.0$ eV (red) and $E_g = 1.5$ eV (blue) are of the same order of magnitude. Same holds for the SLME in the case of $E_g = 1.0$ eV (dashed line). Nevertheless, we like to point out that the SLME does not predict this strong increase in optimal thickness for the last 10% gain of internal luminescence quantum efficiency ($Q_i = 0.9$–1) that is visible in our model (solid lines). As we state above, for the SLME metric, the maximum efficiency for $E_g = 1.5$ eV is reached at infinite thickness and is, therefore, not present in this graph.

To further analyze the impact of the internal luminescence quantum efficiency and the differences between our model and SLME, we plot the maximum efficiency at optimal thickness versus the internal luminescence quantum efficiency in Fig. 4(d). The SLME exhibits a linear decrease in efficiency with decreasing $\ln(Q_i)$ for the entire range of Q_i shown in this graph. Our model shows the same linear decrease only for $Q_i \ll 1$, whereas we see a dramatic drop in maximum efficiency with decreasing Q_i close to the radiative limit of $Q_i = 1$.

As the equations that we use to calculate the maximum efficiency cannot be solved analytically, we use a different approach intuitively to explain the observed dependence of the maximum efficiency on Q_i. For this purpose, we write the efficiency as $\eta = J_{\mathrm{SC}} V_{\mathrm{OC}} \mathrm{FF}/P_{\mathrm{Sun}}$, where P_{Sun} is the power density of the incident sunlight. According to Eq. (1), J_{SC} is independent of the internal luminescence quantum efficiency Q_i. The fill factor FF can also be considered as being almost independent of the internal luminescence quantum efficiency. Therefore, the derivative of η can be approximately calculated via

$$\frac{d\eta}{d\ln(Q_i)} \approx \frac{J_{\mathrm{SC}}\mathrm{FF}}{P_{\mathrm{Sun}}} \frac{dV_{\mathrm{OC}}}{d\ln(Q_i)}. \tag{8}$$

For the SLME metric, J_0 scales with $1/Q_i$, and, consequently, the open-circuit voltage can be written as $V_{\mathrm{OC}} = V_{\mathrm{OC}}^{\mathrm{rad}} + (kT/q)\ln(Q_i)$, where $V_{\mathrm{OC}}^{\mathrm{rad}}$ is the open-circuit voltage in the radiative limit. With these considerations, we can explain the linear increase in efficiency with $\ln(Q_i)$ for the SLMEs (dashed lines) depicted in Fig. 4(d).

For $Q_i = 1$, the SLME limit reaches a value that is between the SQ limit of the band-gap energy E_g and the cutoff energy E_0 and is identical to that predicted by our model (solid lines). However, even small deviations in Q_i away from the radiative limit lead to significant differences in the predicted efficiencies. Following Eq. (24) in Ref. [24], the open-circuit voltage in our model can be written as

$$V_{\mathrm{OC}} = V_{\mathrm{OC}}^{\mathrm{rad}} + \frac{kT}{q}\ln\left(\frac{p_e Q_i}{1+(p_e-1)Q_i}\right), \qquad (9)$$

where p_e denotes the probability of a photon that has been generated by radiative recombination to be emitted. Note that we neglect parasitic absorption here as we do throughout our study.

For $Q_i \ll 1$, the denominator is close to 1, and Eq. (9) simplifies to $V_{\mathrm{OC}} = V_{\mathrm{OC}}^{\mathrm{rad}} + (kT/q)\ln(p_e Q_i)$, implying the same linear increase in efficiency with $\ln(Q_i)$ as in the SLME, whereas the absolute efficiency is overestimated in the SLME by approximately $\Delta\eta = J_{\mathrm{SC}}\mathrm{FF}/P_{\mathrm{Sun}}(kT/q)\ln(p_e)$.

For $Q_i \approx 1$, we cannot neglect the denominator in Eq. (9) anymore, and the open-circuit voltage, and as a result, the efficiency, increase rapidly as Q_i approaches the radiative limit to the same value as predicted by the SLME. Note that the slope in the linear range ($Q_i \ll 1$) is the same for our model and the SLME. The absolute gradient depends on the band-gap energy E_g, as we discuss in the following paragraphs.

Figure 5(a) shows the maximum efficiency versus the internal luminescence quantum efficiency, just like Fig. 4(d), but for various band-gap energies and calculated by our model only. Here, we assume again flat surfaces (for the case of a Lambertian scatterer as the front surface, see Fig. S4 in the Supplemental Material [61]). All absorption coefficients used are defined by Eq. (7) with $E_g =$ 0.7–1.9 eV in steps of 0.2 eV [red to blue, (i)–(viii)], the characteristic energy is $E_{\mathrm{ch}} = 0.5kT$, and the cutoff energies are 0.1 eV below the respective band-gap energies, $E_0 = E_g - 0.1$ eV. The maximum efficiency in the radiative limit is reached for band gaps of 1.3 and 1.5 eV with cutoff energies of 1.2 and 1.4 eV, respectively. This is expected given the band-gap energies of the SQ efficiency maxima plotted in Fig. 3. All curves show the already discussed significant drop in efficiency as Q_i decreases from 100% to 60%. For all $Q_i < 60\%$, the efficiency decreases linearly with decreasing $\ln(Q_i)$ until it asymptotically approaches 0%, as can be surmised for very low Q_i in the case of $E_g = 0.7$ eV (red line).

We concentrate now on the linear slope of $\eta(\ln Q_i)$. Figure 5(b) presents the derivative $[d\eta/d\ln(Q_i)]$ as a function of band-gap energy for $Q_i = 10^{-4}$. This function is almost independent of the assumed light-trapping scheme [61]. A Lambertian light scatterer as the front surface (purple) only slightly deviates from a flat front surface (green) for very low band gaps $E_g < 0.7$ eV. For band-gap energies above

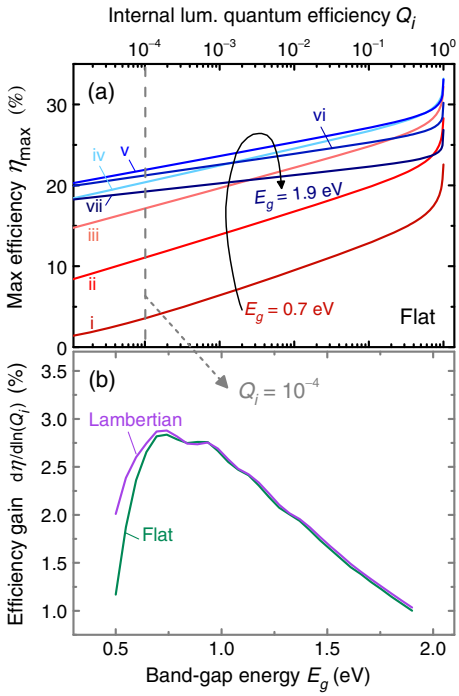

FIG. 5. (a) Maximum efficiency versus internal quantum efficiency Q_i for band gaps $E_g = 0.7$–1.9 eV in steps of 0.2 eV [red to blue, (i)–(vii)] assuming flat devices. Note how both the absolute efficiency for $Q_i = 1$ and the slope of the efficiency depend on E_g. (b) The derivative $d\eta/d\ln(Q_i)$ plotted as a function of E_g for flat surfaces (green) and Lambertian scatterers (purple) at $Q_i = 10^{-4}$.

0.7 eV, the gain in efficiency $[d\eta/d\ln(Q_i)]$ monotonically decreases from 3% to 1% absolute efficiency per decade of internal luminescence quantum efficiency. As the gain in efficiency can be expressed by $[d\eta/d\ln(Q_i)](E_g) \approx J_{\mathrm{SC}}(E_g)\mathrm{FF}(E_g)(kT/qP_{\mathrm{Sun}})$, the shape of the curve $[d\eta/d\ln(Q_i)]$ plotted in Fig. 5(b) can be explained by the dependence of the product $\mathrm{FF}J_{\mathrm{SC}}$ on the band-gap energy E_g. Whereas J_{SC} decreases monotonically with band gap, the fill factor increases strongly for small band gaps and saturates for higher band-gap energies, and the product of these two curves results in the curve of the efficiency gain $[d\eta/d\ln(Q_i)]$, as illustrated in Fig. 5(b).

After discussing the impact of the internal luminescence quantum efficiency and the thickness on the maximum efficiency, we want to close this section by analyzing the effect of the refractive index on the maximal achievable efficiency. For simplicity, we discuss only this for the case of $E_g = 1.5$ eV. The analogous graph for $E_g = 1.0$ eV is displayed in Fig. S5 of the Supplemental Material [61].

Figure 6 illustrates the dependence of the efficiency limit on the refractive index calculated by our model and the SLME model. For $Q_i = 1$ (solid line), there is no difference between our model and the SLME, as is pointed out. The maximum efficiency in the radiative limit is approximately 33.4%, independent of the light-trapping scheme;

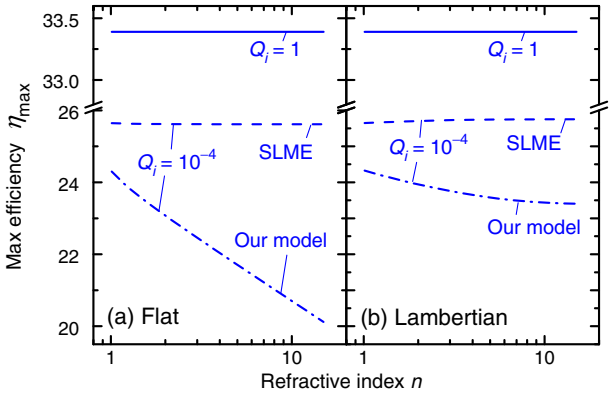

FIG. 6. Dependence of the maximum efficiency η_{max} on the refractive index n for $E_g = 1.5$ eV. In both the radiative limit ($Q_i = 1$, solid lines) and the SLME for $Q_i = 10^{-4}$ (dashed lines), the efficiencies are independent of n. (a) On the other hand, our model (dashed-dotted line) shows a significant efficiency drop of almost 20% as the refractive index n varies from 1 to 10 for flat devices. (b) Assuming a Lambertian scatterer, the refractive index has a much weaker influence of a mere 4%.

see Fig. 6(a) for a flat front surface and Fig. 6(b) for a Lambertian scatterer as a front surface. The value reached is equal to the SQ limit for $E_g = 1.4$ eV, which corresponds to the cutoff energy $E_0 = 1.4$ eV of the examined absorption coefficient. In the SLME, the achievable efficiency is independent of the refractive index, and the texture of the front surface is independent of Q_i. In contrast, our model (dash-dotted line) shows a relative decrease in efficiency of 20% as the refractive index varies from 1 to 10 for flat surfaces. Therefore, the overestimation of the maximum efficiency by SLME increases with increasing refractive index.

The decrease in efficiency with the refractive index in our model is a direct consequence of Eq. (6). The radiative recombination rate R^{rad} is proportional to n^2, and because we hold $Q_i = 10^{-4}$ constant, the nonradiative recombination rate R^{nrad} has to have the same dependence on n as R^{rad} according to Eq. (4). Note that $Q_i = 10^{-4}$ implies $R^{rad} \ll R^{nrad}$. Consequently, the saturation current J_0 increases with n^2, and the efficiency η decreases linearly with $\ln(n)$, as seen in Fig. 6(a) in the case of flat devices. For devices with a Lambertian scatterer as the front surface, the absorption $A(E)$ and, therefore, the short-circuit current J_{SC} are increasing with n. This increase in J_{SC} compensates the increase of J_0 to some extent, and the loss in efficiency with n for fixed $Q_i = 10^{-4}$ is smaller; see dashed-dotted line in Fig. 6(b).

IV. RECIPE TO CALCULATE EFFICIENCY LIMITS

After the detailed discussion of different models and their behavior under certain circumstances, we achieve a deeper understanding of how to calculate a reasonable and also practical efficiency limit from available optical data either gathered by experiments or from electronic structure calculations. Given the strong dependence of the maximum efficiency on the refractive index, we conclude that the real part of the refractive index must not be neglected. Moreover, the calculated efficiency is also very sensitive to the internal luminescence quantum efficiency; see Fig. 5. The internal luminescence quantum efficiency Q_i is a complex interplay between energy levels in the material, defects, and kinetics in the device. It is, therefore, very challenging to determine Q_i computationally, but it might be possible to determine it experimentally without having to fabricate devices [56]. Approaches for first-principles calculations of nonradiative recombination rates due to point defects are emerging [66–68] and could provide in the future at least an estimate of the upper limit of Q_i under idealized situations. In practice, it is useful to treat the internal luminescence quantum efficiency as an independent parameter, in particular, at an early stage of material investigation when materials growth and device fabrication have not yet been optimized. A third point that we want to stress is the thickness dependence of the efficiency. Our results in Sec. III show that a comparison of different materials at a fixed thickness favors certain materials over others without proper justification. Therefore, the optimal thickness should be considered in the figure of merit for all cases with $Q_i < 1$.

We propose to make full use of the available optical data from electronic structure theory to estimate the potential of a new material as follows: (1) Decide on a light-trapping scheme to calculate the absorptance A from the absorption coefficient α; e.g., for flat devices, use Eq. (S1) in the Supplemental Material [61]. (2) Calculate the short-circuit current J_{SC} and the radiative saturation current J_0^{rad} according to Eqs. (1) and (2), which leads to the radiative efficiency limit via Eq. (3). (3) Calculate the absorbance and efficiency for numerous thicknesses to end up with an efficiency-over-thickness curve $\eta(d)$. (4) Find the maximum of this curve $\max[\eta(d)] = \eta(d_{opt})$ and the corresponding optimal thickness d_{opt}. (5) For the reasons stated above, we suggest repeating steps 1–3 for a number of reasonable internal luminescence quantum efficiencies. Note that in the presence of nonradiative recombination ($Q_i \neq 1$), we need in addition to Eqs. (1)–(3) also Eqs. (4)–(6) to determine the efficiency limit. Additionally, we like to point out that this selection metric just like the selection metric from Yu and Zunger can be applied only to materials with a tail slope E_{ch} smaller than kiloteslas; see the Supplemental Material [61].

Exemplarily, we apply the suggested method to a few complex refractive indices that are determined via first-principles calculations. These calculations are performed within the GW approximation [54], as implemented in the VASP code [69,70] and are part of a larger database [71]. A more detailed description of the approach is given in

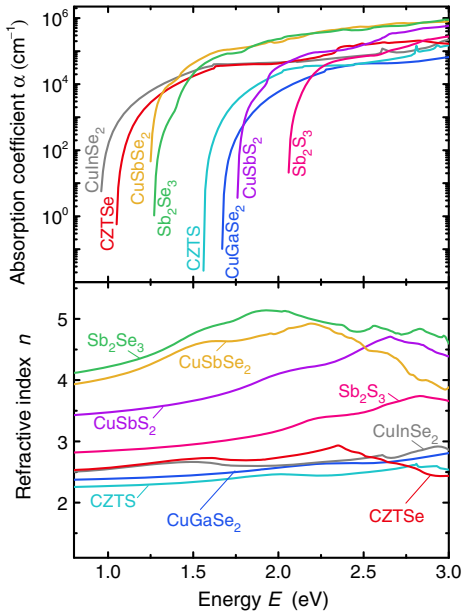

FIG. 7. Absorption coefficient α and refractive index n of $CuInSe_2$ (gray), CZTSe (red), $CuSbSe_2$ (orange), Sb_2Se_3 (green), CZTS (turquoise), $CuGaSe_2$ (blue), $CuSbS_2$ (purple), Sb_2S_3 (pink) as a function of energy as simulated via electronic structure theory.

Refs. [72,73]. For this data set, the dielectric function is calculated in the independent particle approximation. Figure 7 presents the input data in the form of absorption coefficients α and the refractive index n as a function of photon energy E. We apply the method exemplarily to eight materials, namely, $CuInSe_2$ (gray), $Cu_2ZnSnSe_4$ [(CZTSe) red], $CuSbSe_2$ (orange), Sb_2Se_3 (green), CZTS (turquoise), $CuGaSe_2$ (blue), $CuSbS_2$ (purple), and Sb_2S_3 (pink). All these materials have sharp absorption edges with $E_{ch} < kT$, a reasonable absorption coefficient for high energies between 10^5 and 10^6 cm and band-gap energies between 1 and 2 eV. So, at first sight, they are all promising photovoltaic absorber materials.

Figure 8 illustrates the maximum efficiencies calculated according to our method for internal luminescence quantum efficiencies $\ln(Q_i) = 0$ to -7 in steps of -1 (dark to light) sorted by the energy of the direct band gap. In the radiative limit ($Q_i = 1$), the highest efficiencies are reached for CZTSe (red), $CuSbSe_2$ (orange), and Sb_2Se_3 (green). The radiative limit shown in Fig. 8 corresponds well with the maxima of the SQ limit as depicted in Fig. 3, which predicts the highest efficiencies for materials with band-gap energies of 1.1–1.3 eV. Assuming more realistic quantum efficiencies of $Q_i < 10^{-2}$, the highest efficiency is reached for CZTS with a band-gap energy of approximately 1.56 eV. This efficiency maximum is a direct consequence of the band-gap-dependent loss in efficiency due to the internal luminescence quantum efficiency. This effect is addressed in detail in the context of Fig. 5. Note that all these efficiencies

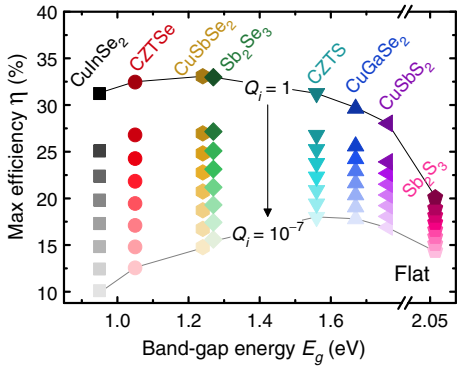

FIG. 8. Maximal efficiencies of eight materials (sorted by direct band gap; see Fig. 6) for different internal quantum efficiencies $\log_{10}(Q_i) = 0$ to -7 in steps of -1 (dark to light colors). For $Q_i = 1$, $CuSbSe_2$ achieves the highest efficiency, whereas for $Q_i < 10^{-2}$, CZTS takes the lead.

are calculated assuming flat devices, with a perfect back reflector and no reflectivity at the front surface.

However, these results are not very conclusive yet. For instance, in the radiative limit, a very weakly absorbing material can outperform other materials with higher absorption if one does not consider the thickness of the device. As the nonradiative recombination in the bulk normally cannot be neglected, the carrier collection efficiency decreases significantly with thickness. Additionally, very thick devices in real life exhibit very low efficiencies due to the finite mobility of the investigated materials. Therefore, in a realistic scenario, we aim for a material that can reach efficiencies as high as possible at a thickness as small as possible.

In Fig. 9, we plot the maximum efficiency over the optimal thickness d_{opt} for the same eight materials (colors and symbols analogous to Fig. 8) to address the importance of thickness to a selection metric. In this case, we exclude the case of $Q_i = 1$, as some of the samples reach their efficiency maximum at infinite thickness for $Q_i = 1$, which is unreasonable for a realistic estimation of the photovoltaic potential of a certain material. For flat surfaces, as shown in Fig. 9(a), $CuSbSe_2$ (orange) exhibits the smallest optimal thicknesses between 600 nm for $Q_i = 10^{-7}$ and 1 μm for $Q_i = 0.1$. In Fig. 9(b), we assume a Lambertian scatterer as the front surface and a perfect flat back reflector. This light-trapping scheme leads to considerably smaller optimal thicknesses and higher efficiencies for all materials. The quantitative gain in efficiency and loss in optimal thickness is, however, distinct for each material. This difference becomes apparent when looking at the variation in optimal thickness between $CuInSe_2$ (gray) and $CuSbS_2$ (purple). For flat devices, the optimal thicknesses for $CuInSe_2$ are on average 5 μm smaller than for $CuSbS_2$. On the other hand, assuming a Lambertian light scatterer, this difference in optimal thickness diminishes, e.g., $d_{opt}(CuSbS_2) < d_{opt}(CuInSe_2)$ for high Q_i and

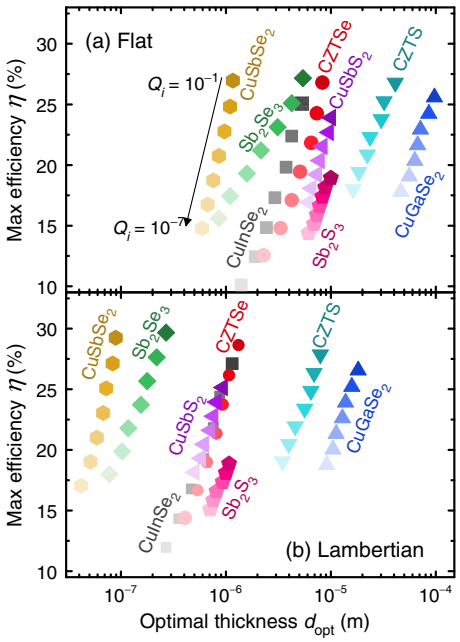

FIG. 9. Efficiency at the optimal thickness for the same materials (see Fig. 7) for internal quantum efficiencies $\log_{10}(Q_i) = -1, -2, -3, -4, -5, -6, -7$ (colors and symbols same as in Fig. 8) with (a) a flat front surface and (b) a Lambertian scatterer as a front surface. For both systems, a perfect flat mirror as a back reflector is assumed.

$d_{opt}(CuSbS_2) > d_{opt}(CuInSe_2)$ for low Q_i. Given this analysis, we conclude that $CuSbSe_2$ reaches the highest efficiencies for the smallest thicknesses and, therefore, is an excellent candidate for a high-performing photovoltaic absorber material based on its complex refractive index.

Given that the materials presented in Figs. 6–8 are all materials that have already been used for photovoltaics, it is worth briefly comparing the results of our assessment based on complex refractive index and internal luminescence quantum efficiency with the empirical results for these technologies. While a technology like $Cu(In, Ga)Se_2$ is capable of achieving efficiencies >22% [74], our analysis for a constant Q_i does not state that this material is superior to the others just based on its complex refractive index. This observation is not particularly surprising given that our selection of materials generally exhibit quite good optical properties for photovoltaic applications. The current lack of success of materials such as CZTSe [75], $CuSbS_2$ [76,77], or $CuSbSe_2$ [78] is a matter of Q_i being lower than for $Cu(In, Ga)Se_2$. Thus, there is a need for computational materials screening to focus on parameters that are related to the presence of defects such as the search for defect-tolerant materials.

V. CONCLUSIONS AND OUTLOOK

The present paper shows that for successful computational screening of prospective photovoltaic materials, a thermodynamically correct translation of material data into photovoltaic output data is mandatory. For this purpose, we define a hierarchy of extension steps (see Fig. 1) that allows us to gradually add physical specifications to the original SQ approach. The first, *impartible* step towards more detail than the band-gap energy embraces knowledge of the complex refractive index of photovoltaic absorber materials as a *necessary* input parameter. As this step deduces the absorptance from the absorption coefficient, assumptions on the device thickness and light-trapping scheme must also be made. The choice of a Lambertian light-trapping scheme as the reference case seems appropriate due to its physical simplicity and practical relevance. The obvious choice for device thickness is then the one that yields the highest efficiency.

The second step towards more detail is the introduction of nonradiative recombination, i.e., the departure from an internal luminescence quantum efficiency $Q_i = 1$. This step necessarily implies that step 1 is conducted correctly. Failure to do so implies misinterpretation of material data, for instance, by neglecting that the internal and external quantum efficiencies differ significantly. The present paper restricts itself to the demonstration of steps 1 and 2. However, the next level of detailing is obviously the departure from virtually infinite mobility; in this case, additional assumptions on junction type and doping densities are necessary [16,17]. It is important to notice that the level of sophistication of such models is still far below that of a specific device model. We are still dealing with generic models and a very low level of computational effort compared to that needed to provide the initial first-principles data.

In view of computational materials screening, the positive message is that the data that are necessary for the first step of detailing are also most easily obtained numerically. However, this does not imply that these properties (absorption coefficient and refractive index) are the most decisive ones. In view of the fact that most practical photovoltaic devices and even most record devices are limited by nonradiative recombination [23,79] urges us to get access to this loss mechanism by first-principles calculations. For instance, the tendency of some types of semiconductors to build shallow instead of deep intrinsic defects [80,81] is certainly an important hint towards prospective photovoltaic performance. Therefore, extending the scope of high-throughput computations to more detailed properties by carefully stepping down the abstraction pyramid (see Fig. 1) will have a high impact on the successful selection and implementation of photovoltaic materials.

ACKNOWLEDGMENTS

The authors thank Urs Aeberhard for a helpful and critical discussion of the manuscript. We acknowledge support from the DFG (Grants No. KI-1571/2-1 and No. RA 473/7-1) and from the Helmholtz Foundation

via the Helmholtz-NREL Solar Energy Initiative. B. B. thanks the Bosch-Forschungsstiftung for a Ph.D. scholarship. S. L. is supported by the U.S. Department of Energy, Office of Science, Basic Energy Sciences, as part of an Energy Frontier Research Center, under Contract No. DE-AC36-08GO28308 to National Renewable Energy Laboratory (NREL).

[1] W. F. Maier, K. Stowe, and S. Sieg, Combinatorial and high-throughput materials science, Angew. Chem., Int. Ed. Engl. **46**, 6016 (2007).
[2] S. Curtarolo, G. L. W. Hart, M. B. Nardelli, N. Mingo, S. Sanvito, and O. Levy, The high-throughput highway to computational materials design, Nat. Mater. **12**, 191 (2013).
[3] A. Jain, S. P. Ong, G. Hautier, W. Chen *et al.*, Commentary: The Materials Project: A materials genome approach to accelerating materials innovation, Appl. Mater. **1**, 011002 (2013).
[4] J. Hachmann, R. Olivares-Amaya, A. Jinich, A. L. Appleton *et al.*, Lead candidates for high-performance organic photovoltaics from high-throughput quantum chemistry – The Harvard Clean Energy Project, Energy Environ. Sci. **7**, 698 (2014).
[5] C. Wadia, A. P. Alivisatos, and D. M. Kammen, Materials availability expands the opportunity for large-scale photovoltaics deployment, Environ. Sci. Technol. **43**, 2072 (2009).
[6] R. E. Brandt, V. Stevanović, D. S. Ginley, and T. Buonassisi, Identifying defect-tolerant semiconductors with high minority-carrier lifetimes: Beyond hybrid lead halide perovskites, MRS Commun. **5**, 265 (2015).
[7] I. E. Castelli, T. Olsen, S. Datta, D. D. Landis, S. Dahl, K. S. Thygesen, and K. W. Jacobsen, Computational screening of perovskite metal oxides for optimal solar light capture, Energy Environ. Sci. **5**, 5814 (2012).
[8] A. J. Lehner, D. H. Fabini, H. A. Evans, C.-A. Hébert, S. R. Smock, J. Hu, H. Wang, J. W. Zwanziger, M. L. Chabinyc, and R. Seshadri, Crystal and electronic structures of complex bismuth iodides $A_3Bi_2I_9$ (A = K, Rb, Cs) related to perovskite: Aiding the rational design of photovoltaics, Chem. Mater. **27**, 7137 (2015).
[9] R. X. Yang, K. T. Butler, and A. Walsh, Assessment of hybrid organic-inorganic antimony sulfides for earth-abundant photovoltaic applications, J. Phys. Chem. Lett. **6**, 5009 (2015).
[10] A. M. Ganose, K. T. Butler, A. Walsh, and D. O. Scanlon, Relativistic electronic structure and band alignment of BiSI, and BiSeI: Candidate photovoltaic materials, J. Mater. Chem. A **4**, 2060 (2016).
[11] M. R. Filip and F. Giustino, Computational screening of homovalent lead substitution in organic-inorganic halide perovskites, J. Phys. Chem. C **120**, 166 (2016).
[12] K. T. Butler, J. M. Frost, J. M. Skelton, K. L. Svane, and A. Walsh, Computational materials design of crystalline solids, Chem. Soc. Rev. **45**, 6138 (2016).
[13] N. M. O'Boyle, C. M. Campbell, and G. R. Hutchison, Computational design and selection of optimal organic photovoltaic materials, J. Phys. Chem. C **115**, 16200 (2011).
[14] A. Yosipof, O. E. Nahum, A. Y. Anderson, H.-N. Barad, A. Zaban, and H. Senderowitz, Data mining and machine learning tools for combinatorial material science of all-oxide photovoltaic cells, Mol. Inform. **34**, 367 (2015).
[15] W. Shockley and H. J. Queisser, Detailed balance limit of efficiency of *p-n* junction solar cells, J. Appl. Phys. **32**, 510 (1961).
[16] J. Mattheis, J. H. Werner, and U. Rau, Finite mobility effects on the radiative efficiency limit of *p-n* junction solar cells, Phys. Rev. B **77**, 085203 (2008).
[17] T. Kirchartz, J. Mattheis, and U. Rau, Detailed balance theory of excitonic and bulk heterojunction solar cells, Phys. Rev. B **78**, 235320 (2008).
[18] T. Tiedje, E. Yablonovitch, G. D. Cody, and B. G. Brooks, Limiting efficiency of silicon solar cells, IEEE Trans. Electron Devices **31**, 711 (1984).
[19] M. A. Green, Limits on the open-circuit voltage and efficiency of silicon solar cells imposed by intrinsic Auger processes, IEEE Trans. Electron Devices **31**, 671 (1984).
[20] T. Kirchartz, F. Staub, and U. Rau, Impact of photon recycling on the open-circuit voltage of metal halide perovskite solar cells, ACS Energy Lett. **1**, 731 (2016).
[21] R. T. Ross, Some thermodynamics of photochemical systems, J. Chem. Phys. **46**, 4590 (1967).
[22] U. Rau, Reciprocity relation between photovoltaic quantum efficiency and electroluminescent emission of solar cells, Phys. Rev. B **76**, 085303 (2007).
[23] M. A. Green, Radiative efficiency of state-of-the-art photovoltaic cells, Prog. Photovoltaics **20**, 472 (2012).
[24] U. Rau, U. W. Paetzold, and T. Kirchartz, Thermodynamics of light management in photovoltaic devices, Phys. Rev. B **90**, 035211 (2014).
[25] K. Vandewal, K. Tvingstedt, A. Gadisa, O. Inganas, and J. V. Manca, On the origin of the open-circuit voltage of polymer-fullerene solar cells, Nat. Mater. **8**, 904 (2009).
[26] J. Yao, T. Kirchartz, M. S. Vezie, M. A. Faist *et al.*, Quantifying Losses in Open-Circuit Voltage in Solution-Processable Solar Cells, Phys. Rev. Applied **4**, 014020 (2015).
[27] C.-H. M. Chuang, A. Maurano, R. E. Brandt, G. W. Hwang, J. Jean, T. Buonassisi, V. Bulović, and M. G. Bawendi, Open-circuit voltage deficit, radiative sub-bandgap states, and prospects in quantum dot solar cells, Nano Lett. **15**, 3286 (2015).
[28] B. Minnaert and M. Burgelman, Efficiency potential of organic bulk heterojunction solar cells, Prog. Photovoltaics **15**, 741 (2007).
[29] H. J. Snaith, Estimating the maximum attainable efficiency in dye-sensitized solar cells, Adv. Funct. Mater. **20**, 13 (2010).
[30] U. Rau, F. Einsele, and G. C. Glaeser, Efficiency limits of photovoltaic fluorescent collectors, Appl. Phys. Lett. **87**, 171101 (2005).
[31] L. J. A. Koster, S. E. Shaheen, and J. C. Hummelen, Pathways to a new efficiency regime for organic solar cells, Adv. Energy Mater. **2**, 1246 (2012).
[32] U. Rau and J. H. Werner, Radiative efficiency limits of solar cells with lateral band-gap fluctuations, Appl. Phys. Lett. **84**, 3735 (2004).

[33] T. Kirchartz, K. Taretto, and U. Rau, Efficiency limits of organic bulk heterojunction solar cells, J. Phys. Chem. C **113**, 17958 (2009).
[34] M. J. Kerr, A. Cuevas, and P. Campbell, Limiting efficiency of crystalline silicon solar cells enhanced to Coulomb-enhanced auger recombination, Prog. Photovoltaics **11**, 97 (2003).
[35] O. D. Miller, E. Yablonovitch, and S. R. Kurtz, Strong internal and external luminescence as solar cells approach the Shockley-Queisser limit, IEEE J. Photovoltaics **2**, 303 (2012).
[36] M. A. Steiner, J. F. Geisz, I. Garcia, D. J. Friedman, A. Duda, and S. R. Kurtz, Optical enhancement of the open-circuit voltage in high quality GaAs solar cells, J. Appl. Phys. **113**, 123109 (2013).
[37] L. P. Yu and A. Zunger, Identification of Potential Photovoltaic Absorbers Based on First-Principles Spectroscopic Screening of Materials, Phys. Rev. Lett. **108**, 068701 (2012).
[38] C. N. Savory, A. Walsh, and D. O. Scanlon, Can Pb-free halide double perovskites support high-efficiency solar cells?, ACS Energy Lett. **1**, 949 (2016).
[39] A. Zakutayev, X. W. Zhang, A. Nagaraja, L. P. Yu, S. Lany, T. O. Mason, D. S. Ginley, and A. Zunger, Theoretical prediction and experimental realization of new stable inorganic materials using the inverse design approach, J. Am. Chem. Soc. **135**, 10048 (2013).
[40] L. P. Yu, R. S. Kokenyesi, D. A. Keszler, and A. Zunger, Inverse design of high absorption thin-film photovoltaic materials, Adv. Energy Mater. **3**, 43 (2013).
[41] C. N. Savory, A. M. Ganose, W. Travis, R. S. Atri, R. G. Palgrave, and D. O. Scanlon, An assessment of silver copper sulfides for photovoltaic applications: Theoretical and experimental insights, J. Mater. Chem. A **4**, 12648 (2016).
[42] T. Yokoyama, F. Oba, A. Seko, H. Hayashi, Y. Nose, and I. Tanaka, Theoretical photovoltaic conversion efficiencies of $ZnSnP_2$, $CdSnP_2$, and $Zn_{1-x}Cd_xSnP_2$ alloys, Appl. Phys. Express **6**, 061201 (2013).
[43] I.-H. Lee, J. Lee, Y. J. Oh, S. Kim, and K. Chang, Computational search for direct band gap silicon crystals, Phys. Rev. B **90**, 115209 (2014).
[44] Y. J. Oh, I.-H. Lee, S. Kim, J. Lee, and K. J. Chang, Dipole-allowed direct band gap silicon superlattices, Sci. Rep. **5**, 18086 (2015).
[45] W.-J. Yin, T. Shi, and Y. Yan, Superior photovoltaic properties of lead halide perovskites: Insights from first-principles theory, J. Phys. Chem. C **119**, 5253 (2015).
[46] M. Bercx, N. Sarmadian, R. Saniz, B. Partoens, and D. Lamoen, First-principles analysis of the spectroscopic limited maximum efficiency of photovoltaic absorber layers for CuAu-like chalcogenides and silicon, Phys. Chem. Chem. Phys. **18**, 20542 (2016).
[47] W. Meng, B. Saparov, F. Hong, J. Wang, D. B. Mitzi, and Y. Yan, Alloying and defect control within chalcogenide perovskites for optimized photovoltaic application, Chem. Mater. **28**, 821 (2016).
[48] N. Sarmadian, R. Saniz, B. Partoens, and D. Lamoen, First-principles study of the optoelectronic properties and photovoltaic absorber layer efficiency of Cu-based chalcogenides, J. Appl. Phys. **120**, 085707 (2016).
[49] J. Heo, R. Ravichandran, C. F. Reidy, J. Tate, J. F. Wager, and D. A. Keszler, Design meets nature: Tetrahedrite solar absorbers, Adv. Energy Mater. **5**, 1401506 (2015).
[50] R. Brendel and R. Peibst, Contact selectivity and efficiency in crystalline silicon photovoltaics, IEEE J. Photovoltaics **6**, 1413 (2016).
[51] T. Tiedje, E. Yablonovitch, G. D. Cody, and B. G. Brooks, Limiting efficiency of silicon solar cells, IEEE Trans. Electron Devices **31**, 711 (1984).
[52] A. Marti, J. L. Balenzategui, and R. F. Reyna, Photon recycling and Shockley's diode equation, J. Appl. Phys. **82**, 4067 (1997).
[53] T. Kirchartz and U. Rau, Decreasing radiative recombination coefficients via an indirect band gap in lead halide perovskites, J. Phys. Chem. Lett. **8**, 1265 (2017).
[54] L. Hedin, New method for calculating 1-particle Greens function with application to electron-gas problem, Phys. Rev. **139**, A796 (1965).
[55] A. Richter, M. Hermle, and S. W. Glunz, Reassessment of the limiting efficiency for crystalline silicon solar cells, IEEE J. Photovoltaics **3**, 1184 (2013).
[56] F. Staub, H. Hempel, J.-C. Hebig, J. Mock, U. W. Paetzold, U. Rau, T. Unold, and T. Kirchartz, Beyond Bulk Lifetimes: Insights into Lead Halide Perovskite Films from Time-Resolved Photoluminescence, Phys. Rev. Applied **6**, 044017 (2016).
[57] http://rredc.nrel.gov/solar/spectra/am1.5/astmg173/astmg173.html.
[58] Alternatively, one can explain the perfect charge-carrier collection by an infinite charge-carrier mobility combined with a finite thickness. However, this explanation still leads to a contradiction in the assumptions, as the device has to be infinitely thick for the steplike absorption.
[59] U. Aeberhard, Quantum-kinetic theory of steady-state photocurrent generation in thin films: Coherent versus incoherent coupling, Phys. Rev. B **89**, 115303 (2014).
[60] U. Aeberhard and U. Rau, Microscopic Perspective on Photovoltaic Reciprocity in Ultrathin Solar Cells, Phys. Rev. Lett. **118**, 247702 (2017).
[61] See the Supplemental Material at http://link.aps.org/supplemental/10.1103/PhysRevApplied.8.024032 for a more detailed explanation of the light-trapping schemes.
[62] M. A. Green, Lambertian light trapping in textured solar cells and light-emitting diodes: Analytical solutions, Prog. Photovoltaics **10**, 235 (2002).
[63] S. M. Sze, *Physics of Semiconductor Devices* (John Wiley & Sons, New York, 1936).
[64] F. Urbach, The long-wavelength edge of photographic sensitivity and of the electronic absorption of solids, Phys. Rev. **92**, 1324 (1953).
[65] S. De Wolf, J. Holovsky, S.-J. Moon, P. Löper, B. Niesen, M. Ledinsky, F.-J. Haug, J.-H. Yum, and C. Ballif, Organometallic halide perovskites: Sharp optical absorption edge and its relation to photovoltaic performance, J. Phys. Chem. Lett. **5**, 1035 (2014).
[66] A. Alkauskas, Q. Yan, and C. G. Van de Walle, First-principles theory of nonradiative carrier capture via multiphonon emission, Phys. Rev. B **90**, 075202 (2014).

[67] L. Shi, K. Xu, and L.-W. Wang, Comparative study of *ab initio* nonradiative recombination rate calculations under different formalisms, Phys. Rev. B **91**, 205315 (2015).
[68] G. D. Barmparis, Y. S. Puzyrev, X. G. Zhang, and S. T. Pantelides, Theory of inelastic multiphonon scattering and carrier capture by defects in semiconductors: Application to capture cross sections, Phys. Rev. B **92**, 214111 (2015).
[69] G. Kresse and D. Joubert, From ultrasoft pseudopotentials to the projector augmented-wave method, Phys. Rev. B **59**, 1758 (1999).
[70] M. Shishkin and G. Kresse, Implementation and performance of the frequency-dependent GW method within the PAW framework, Phys. Rev. B **74**, 035101 (2006).
[71] https://materials.nrel.gov.
[72] S. Lany, Band-structure calculations for the 3*d* transition metal oxides in GW, Phys. Rev. B **87**, 085112 (2013).
[73] S. Lany, Semiconducting transition metal oxides, J. Phys. Condens. Matter **27**, 283203 (2015).
[74] P. Jackson, R. Wuerz, D. Hariskos, E. Lotter, W. Witte, and M. Powalla, Effects of heavy alkali elements in $Cu(In,Ga)Se_2$ solar cells with efficiencies up to 22.6%, Phys. Status Solidi RRL **10**, 583 (2016).
[75] W. Wang, M. T. Winkler, O. Gunawan, T. Gokmen, T. K. Todorov, Y. Zhu, and D. B. Mitzi, Device characteristics of CZTSSe thin-film solar cells with 12.6% efficiency, Adv. Energy Mater. **4**, 1301465 (2014).
[76] F. W. de Souza Lucas, A. W. Welch, L. L. Baranowski, P. C. Dippo *et al.*, Effects of thermochemical treatment on $CuSbS_2$ photovoltaic absorber quality and solar cell reproducibility, J. Phys. Chem. C **120**, 18377 (2016).
[77] A. W. Welch, L. L. Baranowski, P. Zawadzki, C. DeHart, S. Johnston, S. Lany, C. A. Wolden, and A. Zakutayev, Accelerated development of $CuSbS_2$ thin film photovoltaic device prototypes, Prog. Photovoltaics **24**, 929 (2016).
[78] A. W. Welch, L. L. Baranowski, P. Zawadzki, S. Lany, C. A. Wolden, and A. Zakutayev, $CuSbSe_2$ photovoltaic devices with 3% efficiency, Appl. Phys. Express **8**, 082301 (2015).
[79] U. Rau, B. Blank, T. C. M. Muller, and T. Kirchartz, Efficiency Potential of Photovoltaic Materials and Devices Unveiled by Detailed-Balance Analysis, Phys. Rev. Applied **7**, 044016 (2017).
[80] R. E. Brandt, V. Stevanovic, D. S. Ginley, and T. Buonassisi, Identifying defect-tolerant semiconductors with high minority-carrier lifetimes: Beyond hybrid lead halide perovskites, MRS Commun. **5**, 265 (2015).
[81] W.-J. Yin, T. Shi, and Y. Yan, Unusual defect physics in $CH_3NH_3PbI_3$ perovskite solar cell absorber, Appl. Phys. Lett. **104**, 063903 (2014).